Available online at www.sciencedirect.com
SCIENCE DIRECT®
Journal of Solid State Chemistry 172 (2003) 464–470
JOURNAL OF SOLID STATE CHEMISTRY
http://elsevier.com/locate/jssc

Hydrothermal synthesis and characterization of layered vanadium phosphite: $[HN(C_2H_4)_3N][(VO)_2(HPO_3)_2(OH)(H_2O)] \cdot H_2O$

Zhan Shi, Dong Zhang, Guanghua Li, Lei Wang, Xiaoying Lu, Jia Hua, and Shouhua Feng*

State Key Laboratory of Inorganic Synthesis and Preparative Chemistry, College of Chemistry, Jilin University, Changchun 130023, China

Received 27 September 2002; received in revised form 7 December 2002; accepted 14 December 2002

Abstract

A novel compound, $[HN(C_2H_4)_3N][(VO)_2(HPO_3)_2(OH)(H_2O)] \cdot H_2O$, was hydrothermally synthesized and characterized by single crystal X-ray diffraction. This compound crystallizes in the monoclinic system with the space group $C2/c$ and cell parameters $a = 11.0753(3)$ Å, $b = 17.8265(6)$ Å, $c = 16.5229(5)$ Å, and $\beta = 92.362(2)^\circ$. The structure of the compound consists of vanadium phosphite layers which are built up from the infinite one-dimensional chains of $[(VO)(H_2O)(HPO_3)_2]^{2-}$ of octahedral $VO_5(H_2O)$ and pseudo pyramidal $[HPO_3]$, and bridging binuclear fragments of $[VO(OH)]_2$. Thermogravimetric analysis and magnetic susceptibility data for this compound are given.

Keywords: Hydrothermal synthesis; Vanadium phosphite; Layered structure

1. Introduction

Open-framework metal phosphates such as microporous and layered aluminophosphates have shown potential applications in the fields of catalysis, ion exchange, adsorption and host–guest assembly [1,2]. The diversity in crystal architectures of metal phosphates was mainly derived from the utility of various organic templates and the substitution of metal ions such as transition metal ions for Al ions. In the creation of new structures of open-framework metal phosphates, few examples were taken account for the replacement of phosphate by phosphite, although the incorporations of the pseudo-pyramidal hydrogen phosphite group $[HPO_3]^{2-}$ into the desired structures were reported in several simple organically templated cobalt phosphite [3], manganese phosphite [4,5], zinc phosphites [6–11], and two vanadium phosphites, $[HN(CH_3)(CH_2CH_2)N(CH_3)H][(VO_4)(OH)_2(HPO_3)_4]$ and $[H_2N(CH_2\ CH_2)_2NH_2][(VO)_3(HPO_3)_4(H_2O)]$ [12]. Apparently, organically templated metal phosphites reserve much room for novel open-framework crystals, just like the extensively studied metal phosphates, in which numerous novel structures with one-, two-, and three-dimensional frameworks have been discovered for years [13–16]. Our motivation for searching for novel open-framework phosphites is based on the utility of organic template, 1,4-diazabicyclo [2,2,2] octane (DABCO) in the hydrothermal systems of vanadium phosphates. DABCO has been found as a template for directing three novel vanadium phosphates, $[HN(C_2H_4)_3NH]_2[(VO)_8(HPO_4)_3(PO_4)_4(OH)_2] \cdot 2H_2O$, $[HN(C_2H_4)_3NH][(VO)_3(OH)_2(PO_4)_2]$ [17], and $[HN(C_2H_4)_3NH]K_{1.35}[V_5O_9(PO_4)_2] \cdot xH_2O$ [18], and the variety for vanadium coordination states such as tetrahedral, square pyramidal, trigonal bipyramidal and octahedral arrangements in the vanadium phosphates has been evidenced.

In this paper, we report the synthesis, crystal structure, thermal and magnetic properties of a novel vanadium phosphite, $[HN(C_2H_4)_3N][(VO)_2(HPO_3)_2(OH)(H_2O)] \cdot H_2O$, which is synthesized by hydrothermal method in the presence of DABCO.

2. Experimental

2.1. Synthesis and characterization

The title compound was prepared from a reaction mixture of vanadium oxide (V_2O_5), phosphorous acid

*Corresponding author. Fax: +86-431-5671-974.
E-mail address: shfeng@mail.jlu.edu.cn (S. Feng).

0022-4596/03/$ - see front matter © 2003 Elsevier Science (USA). All rights reserved.
doi:10.1016/S0022-4596(03)00037-9

(H_3PO_3), DABCO, boric acid (H_3BO_3) and distilled water with a molar ratio of 1.0 V_2O_5:10.0 H_3PO_3:10.0 DABCO:10.0 H_3BO_3:222 H_2O. A typical procedure began with mixing 0.091 g V_2O_5, 1.100 g DABCO, 0.310 g H_3BO_3 and 0.410 g H_3PO_3 with 2 ml H_2O to form a reaction mixture. The mixture was heated in a sealed Teflon-lined steel autoclave at 160°C for 120 h. The resulting blue crystals were washed with distilled water, filtered and dried in air. The yield of product was 60% in weight based on vanadium.

X-ray powder diffraction (XRD) data were collected on a Siemens D5005 diffractometer with Cu$K\alpha$ radiation ($\lambda = 1.5418$ Å). The step size was 0.02° and the count time was 4 s. The elemental analysis was conducted on a Perkin–Elmer 2400 elemental analyzer. Inductively coupled plasma (ICP) analysis was performed on a Perkin–Elmer Optima 3300DV ICP instrument. The infrared (IR) spectrum was recorded within the 400–4000 cm^{-1} region on a Nicolet Impact 410 FTIR spectrometer using KBr pellets. A Perkin–Elmer DTA 1700 differential thermal analyzer was used to obtain the differential thermal analysis (DTA) and a Perkin–Elmer TGA 7 thermogravimetric analyzer to obtain thermogravimetric analysis (TGA) curves in an atmospheric environment with a heating rate of 10°C min^{-1}.

ESR spectra at room temperature were recorded on a Bruker ESR 300 spectrometer. Magnetic susceptibility data were collected based on a 0.049 g sample over the temperature range 4–298 K at a magnetic field of 5 kG on a Quantum Design MPMS-7 SQUID magnetometer.

2.2. Determination of crystal structure

A suitable blue single crystal with dimensions $0.20 \times 0.15 \times 0.15$ mm was glued to a thin glass fiber and mounted on a Siemens Smart CCD diffractometer equipped with a normal-focus, 2.4-kW sealed-tube X-ray source (graphite-monochromatic Mo$K\alpha$ radiation ($\lambda = 0.71073$ Å)) operating at 50 kV and 40 mA. Intensity data were collected at a temperature of 20 ± 2°C. Date processing was accomplished with the SAINT processing program [19]. The total numbers of measured reflections and observed unique reflections were 6176 and 2080, respectively. Intensity data of 992 independent reflections ($-12 \leqslant h \leqslant 12$, $-18 \leqslant k \leqslant 19$, $-18 \leqslant l \leqslant 17$) were collected in the ω scan mode. An empirical absorption correction was applied using the SADABS program with $T_{min} = 0.448$ and $T_{max} = 0.602$. The structure was solved in the space group $C2/c$ by direct methods and refined on F^2 by full-matrix least-squares using SHELXTL97. The phosphorous and vanadium atoms were located first. Carbon, nitrogen, and oxygen were then found in the difference Fourier map. Difference Fourier maps also showed a significant region ($>2e/Å^3$) of electron density close to the P(2) species. A disordering effect of the P(2) atom over two adjacent positions with occupancy of 0.7 and 0.3 was therefore modeled. Hydrogen atoms were placed geometrically and located in the difference Fourier map. All non-hydrogen atoms were refined with anisotropic thermal parameters. A summary of the crystallographic data is presented in Table 1.

3. Results and discussion

3.1. Characterization

ICP analysis for the product gave the contents of V 22.26 wt% (calcd. 22.14 wt%) and P 13.39% (calcd. 13.46 wt%), indicating a V:P ratio of 1:1. Elemental analysis showed that the sample contains 15.56, 4.27 and 6.15 wt% of C, H and N, respectively, in agreement with the expected values of 15.66, 4.38 and 6.09 wt% of C, H and N on the basis of the empirical formula given by the single-crystal structure analysis.

Thermogravimetic analysis (Fig. 1) indicated the weight loss of the sample ca. 7.17% in the temperature range from 100°C to 160°C, consistent with the loss of water, and the weight loss of 25.65% from 300°C to 780°C, corresponding to the decomposition of DABCO template (calcd. 24.82%). Accordingly, the DTA curve exhibited one endothermic and two exothermic peaks for the loss of water and the decomposition of the

Table 1
Crystal data and structural refinement for $[HN(C_2H_4)_3N][(VO)_2(HPO_3)_2(OH)(H_2O)] \cdot H_2O$

Empirical formula	$C_6H_{20}N_2V_2P_2O_{11}$
Formula weight	460.06
Temperature	293(2) K
Wavelength	0.71073 Å
Crystal system	Monoclinc
Space group	$C2/c$
Unit cell dimensions	$a = 11.0753(3)$ Å
	$b = 17.8265(6)$ Å
	$c = 16.5229(5)$ Å
	$\beta = 92.362(2)$°
Volume	3259.41(17) $Å^3$
Z	8
Calculated density	1.875 Mg m^{-3}
Absorption coefficient	1.399 mm^{-1}
$F(000)$	1872
Crystal size	$0.400 \times 0.300 \times 0.300$ mm^3
Reflections collected/unique	6176/2080 [R(int) = 0.0257]
Data/restraints/parameter	2080/4/229
Goodness-of-fit on F^2	1.036
Final R indices [$I > 2\sigma(I)$]*	$R_1 = 0.0410$, $wR_2 = 0.1025$
R indices (all data)	$R_1 = 0.0484$, $wR_2 = 0.1066$
Largest diff. peak and hole	1.902 and $-0.652e$ $Å^{-3}$

Note. $R_1 = \sum ||F_o| - |F_c|| / \sum |F_o|$; $wR_2 = \sum [w(F_o^2 - F_c^2)^2] / \sum [w(F_o^2)]^2 1/2$; $w = 1/[\sigma^2 |F_o|^2 + (0.0511P)^2 + 19.56P]$, where $P = [|F_o|^2 + 2|F_c|^2]/3$.

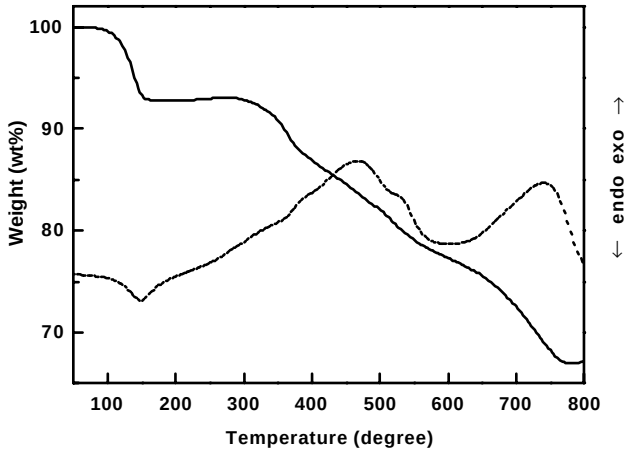

Fig. 1. TG-DTA curves of the vanadium phosphite.

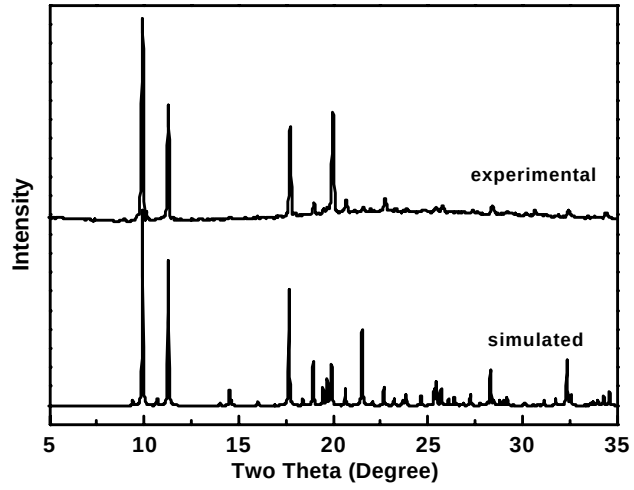

Fig. 2. Experimental and simulated power X-ray diffraction patterns for $[HN(C_2H_4)_3N][(VO)_2(HPO_3)_2(OH)(H_2O)]\cdot H_2O$.

organic template in air, respectively. The structure was collapsed at 300°C when the organic was lost.

Powder X-ray diffraction pattern for $[HN(C_2H_4)_3N][(VO)_2(HPO_3)_2(OH)(H_2O)]\cdot H_2O$ was consistent with the simulated one on the basis of the single-crystal structure, as shown in Fig. 2 [20]. The diffraction peaks on both patterns corresponded well in position, indicating the phase purity of the as-synthesized sample. The difference in reflection intensities between the simulated and experimental patterns was due to the variation in crystal orientation for the power sample.

IR spectrum of the sample showed that the large band at 3421 cm^{-1} arises from O–H and N–H stretching vibrations, and the intense bands at 1112 and 997 cm^{-1} were associated with the stretching vibrations of V–O and P–O bonds, respectively. There appeared the absorptions at 2408 cm^{-1} as well due to the stretching vibrations of the H–P groups in phosphite anions.

X-bond ESR spectra of the sample were recorded on powdered sample at room temperature. The spectra showed isotropic signals with a "g"-value of 1.9562, which clearly indicated the existence of vanadium (IV) ions in the compound.

3.2. Description of structure

The structure of the compound consists of V–O–P layers, as in many layered inorganic/organic vanadium phosphates, the interlamellar space of which is occupied by water molecules and monoprotonated DABCO cations. An ORTEP drawing of the asymmetric unit of the structure is shown in Fig. 3. Atomic positions and thermal parameters are provided in Table 2. Selected bond distance and angles are listed in Table 3.

In this structure, two independent vanadium atoms present two different coordination geometries. The

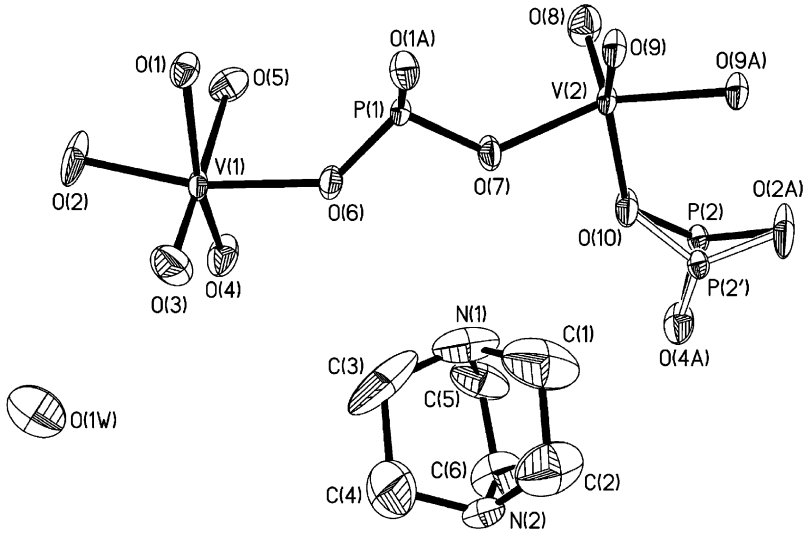

Fig. 3. ORTEP view of the structure of the vanadium phosphite, showing the atom-labeling scheme (50% thermal ellipsoids).

Table 2
Atomic coordinates ($\times 10^4$) and equivalent isotropic displacement parameters ($Å^2 \times 10^3$) for $[HN(C_2H_4)_3N][(VO)_2(HPO_3)_2(OH)(H_2O)] \cdot H_2O$

Atom	x	y	z	U (eq)
V(1)	6207(1)	2896(1)	3727(1)	19(1)
V(2)	743(1)	3901(1)	3320(1)	16(1)
P(1)	3559(1)	3541(1)	3127(1)	15(1)
P(2)	−982(2)	3105(1)	4606(1)	16(1)
P(2′)	−937(4)	2811(3)	4390(3)	16(1)
O(1)	6419(3)	3591(2)	2787(2)	23(1)
O(2)	7963(3)	3095(3)	4003(2)	56(1)
O(3)	6386(4)	2090(2)	3334(3)	45(1)
O(4)	5889(3)	2578(2)	4868(2)	40(1)
O(5)	6009(3)	4020(2)	4369(2)	34(1)
O(6)	4412(3)	2983(2)	3531(2)	24(1)
O(7)	2296(3)	3351(2)	3418(2)	25(1)
O(8)	1037(3)	4703(2)	3712(2)	36(1)
O(9)	919(3)	3942(2)	2151(2)	21(1)
O(10)	200(3)	3205(2)	4160(2)	31(1)
O(1W)	8028(5)	888(3)	3942(3)	65(1)
N(1)	2400(8)	1750(4)	3770(3)	63(2)
N(2)	1977(4)	382(2)	3929(3)	35(1)
C(1)	1464(11)	1534(5)	3159(5)	85(3)
C(2)	1249(9)	702(5)	3257(5)	79(2)
C(3)	3479(11)	1340(7)	3632(6)	96(4)
C(4)	3249(8)	487(5)	3765(7)	87(3)
C(5)	2085(7)	1613(4)	4595(4)	55(2)
C(6)	1726(7)	804(4)	4659(4)	56(2)
H(1A)	1731	1641	2619	80
H(1B)	725	1811	3240	80
H(2A)	401	617	3349	80
H(2B)	1440	447	2760	80
H(3A)	4124	1511	4002	80
H(3B)	3725	1425	3083	80
H(4A)	3450	207	3286	80
H(4B)	3751	306	4219	80
H(5A)	1419	1935	4737	80
H(5B)	2769	1719	4963	80
H(6A)	2162	579	5119	80
H(6B)	869	774	4755	80
H(1)	2430	2210	3670	80
H(9)	1480	3720	1880	80
H(1WA)	7370	920	4250	80
H(1WB)	8130	360	3910	80
H(51)	6220	4010	4880	80
H(52)	6210	4440	4210	80

Note. U(eq) is defined as one-third of the trace of the orthogonalized U_{ij} tensor.

Table 3
Selected bond lengths (Å) and angles (°) for $[HN(C_2H_4)_3N][(VO)_2(HPO_3)_2(OH)(H_2O)] \cdot H_2O$

V(1)–O(1)	2.007(3)	P(1)–O(1)#2	1.514(3)
V(1)–O(2)	2.010(4)	P(1)–O(6)	1.508(3)
V(1)–O(3)	1.593(4)	P(1)–O(7)	1.535(3)
V(1)–O(4)	2.013(3)	P(2)–O(2)#4	1.503(4)
V(1)–O(5)	2.282(4)	P(2)–O(4)#3	1.498(4)
V(1)–O(6)	2.008(3)	P(2)–O(10)	1.538(4)
V(2)–O(7)	1.981(3)	N(1)–C(1)	1.469(11)
V(2)–O(8)	1.597(4)	N(1)–C(3)	1.427(16)
V(2)–O(9)	1.952(3)	N(1)–C(5)	1.443(10)
V(2)–O(9)#1	1.970(3)	N(2)–C(2)	1.461(10)
V(2)–O(10)	1.974(3)	N(2)–C(4)	1.457(10)
C(1)–C(2)	1.512(13)	N(2)–C(6)	1.459(8)
C(5)–C(6)	1.499(11)	C(3)–C(4)	1.559(16)
O(3)–V(1)–O(1)	102.72(17)	O(8)–V(2)–O(9)	109.91(17)
O(3)–V(1)–O(6)	98.20(18)	O(8)–V(2)–O(9)#1	107.39(16)
O(1)–V(1)–O(6)	88.48(12)	O(9)–V(2)–O(9)#1	74.77(15)
O(3)–V(1)–O(2)	96.7(2)	O(8)–V(2)–O(10)	109.97(18)
O(1)–V(1)–O(2)	85.67(14)	O(9)–V(2)–O(10)	139.91(15)
O(6)–V(1)–O(2)	164.90(19)	O(9)#1–V(2)–O(10)	89.66(13)
O(3)–V(1)–O(4)	99.1(2)	O(8)–V(2)–O(7)	104.37(16)
O(1)–V(1)–O(4)	158.22(16)	O(9)–V(2)–O(7)	88.68(13)
O(6)–V(1)–O(4)	87.86(13)	O(9)#1–V(2)–O(7)	147.60(14)
O(2)–V(1)–O(4)	92.42(14)	O(10)–V(2)–O(7)	85.41(13)
O(3)–V(1)–O(5)	176.16(19)	O(8)–V(2)–V(2)#1	116.38(13)
O(1)–V(1)–O(5)	80.50(14)	O(9)–V(2)–V(2)#1	37.68(9)
O(6)–V(1)–O(5)	83.90(13)	O(9)#1–V(2)–V(2)#1	37.26(9)
O(2)–V(1)–O(5)	81.42(19)	O(10)–V(2)–V(2)#1	116.53(10)
O(4)–V(1)–O(5)	77.77(16)	O(7)–V(2)–V(2)#1	119.80(10)
O(6)–P(1)–O(1)#2	116.35(17)	O(4)#3–P(2)–O(2)#4	114.0(3)
O(6)–P(1)–O(7)	106.13(17)	O(4)#3–P(2)–O(10)	109.4(2)
O(1)#2–P(1)–O(7)	112.21(17)	O(2)#4–P(2)–O(10)	109.8(2)
P(1)#2–O(1)–V(1)	138.0(2)	P(1)–O(7)–V(2)	131.62(19)
P(2)#5–O(2)–V(1)	150.5(2)	V(2)–O(9)–V(2)#1	105.06(14)
P(2)#3–O(4)–V(1)	139.7(3)	P(2)–O(10)–V(2)	134.3(2)
P(1)–O(6)–V(1)	136.11(19)		

Note. Symmetry transformations used to generate equivalent atoms: #1, $-x$, y, $-z+1/2$; #2, $-x+1$, y, $-z+1/2$; #3, $-x+1/2$, $-y+1/2$, $-z+1$; #4, $x-1$, y, z; #5, $x+1$, y, z.

six-coordinated vanadium site V(1) exhibits the distorted octahedral geometry with the basal positions defined by oxygen donors from each of four adjacent phosphite groups and the apical position by the terminal oxide group and one water molecule. The water molecule O(5), weakly bonded with V(1) (2.282 Å), is opposite to the classical short-bond V = O(3) (1.593 Å). The coordination of V(2) square pyramid is defined by the terminal oxygen group (V = O(8), 1.597 Å), two oxygen donors from two phosphite groups (V–O(7), 1.981 Å; V–O(10), 1.974 Å), and two bridging hydroxy groups (V–O(9), 1.952 or 1.970 Å). Both of the two phosphite groups adopt the μ_3-coordination mode. The atom P(1) has its two oxygen atoms (O(1) and O(6)) linking two V(1) and one oxygen atom O(7) bonded to V(2). The atom P(2) has the same coordination environment as that of the atom P(1). The atom P(2) has its three oxygen atoms bonded to two V(1) and one V(2). Thus, the infinite V/P/O layer is constructed from these VO_6 octahedra, VO_5 square pyramids and $[HPO_3]^{2-}$ pseudo-pyramidal units. A view of the structure perpendicular to the plane of the layer orientated in the [010] plane is shown in Fig. 4(a). Bond-length and bond-strength calculations were based on the method and data from Brown and Shannon [21] and Brown and Altermatt [22]. The bond valence sums (BVS) calculations assuming V(1) and V(2) bonds gave the values of 4.11 and 4.08, respectively. ESR and magnetic measurement supported the BVS calculations.

The layer with the composition of $[(VO)(H_2O)(VO)(OH)(HPO_3)_2]^-$ is constructed by connecting $[(VO)(H_2O)(HPO_3)_2]^{2-}$ chains through bridging binuclear $[VO(OH)]_2$ fragments. The chains are composed of vertex-sharing $[VO_5(H_2O)]$ octahedral and $[HPO_3]$ pseudo-pyramidal fused together via V–O–P bonds. Each $[VO_5(H_2O)]$ group forms four V–O–P links, resulting in polyhedral "four-rings" with strict alternation of the V and P species. Based on the V(1) configuration, a pair of the short V(1) = O(3) bonds project from alternate sides of the chains in an ordered fashion. The polyhedral chain-linkage pattern of vertex-linked $[VO_5(H_2O)]/[HPO_3]$ four-rings is similar to that found in $[CN_3H_6][VO(H_2O)(HPO_4)(H_2PO_4)]\cdot H_2O$ [15], $Ba_2VO(PO_4)_2\cdot H_2O$ [23] and $VO(H_2PO_4)_2\cdot H_2O$ [24] with one-dimensional chain structure. This binuclear structural unit consists of two $[VO_5]$ square pyramids, corner-sharing through hydroxide {V(2)–O(H)–V(2)} interactions. Each binuclear unit links two $[(VO)(H_2O)(HPO_3)_2]^{2-}$ chains through four phosphite groups to form the layers with the composition of $[(VO)(H_2O)(VO)(OH)(HPO_3)_2]^-$ in the *ac*-plane as shown in Fig. 4(a). It is noteworthy that, unlike other layered vanadium phosphates or vanadium phosphites, these layers in our compound are wave like (as seen in Fig. 5). This vanadium phosphite layer is similar to that in the vanadium phosphate, $[(NH_3C_3H_6)NH(C_2H_4)_2NH(C_3H_6NH_3)][(VO)_5(OH)_2(PO_4)_4]\cdot 2H_2O$ [23]. As shown in Fig. 4(b), the layer in the later compound possesses two units: the binuclear $[VO(OH)]_2$ fragment, the same as the title compound, and the $[(VO)_3(PO_4)_4]$ chain, different from the $[(VO)(H_2O)(HPO_3)_2]$ chain in our compound. Obviously, the structural differences between the phosphite and the phosphate result from the fact that phosphite groups adopt the

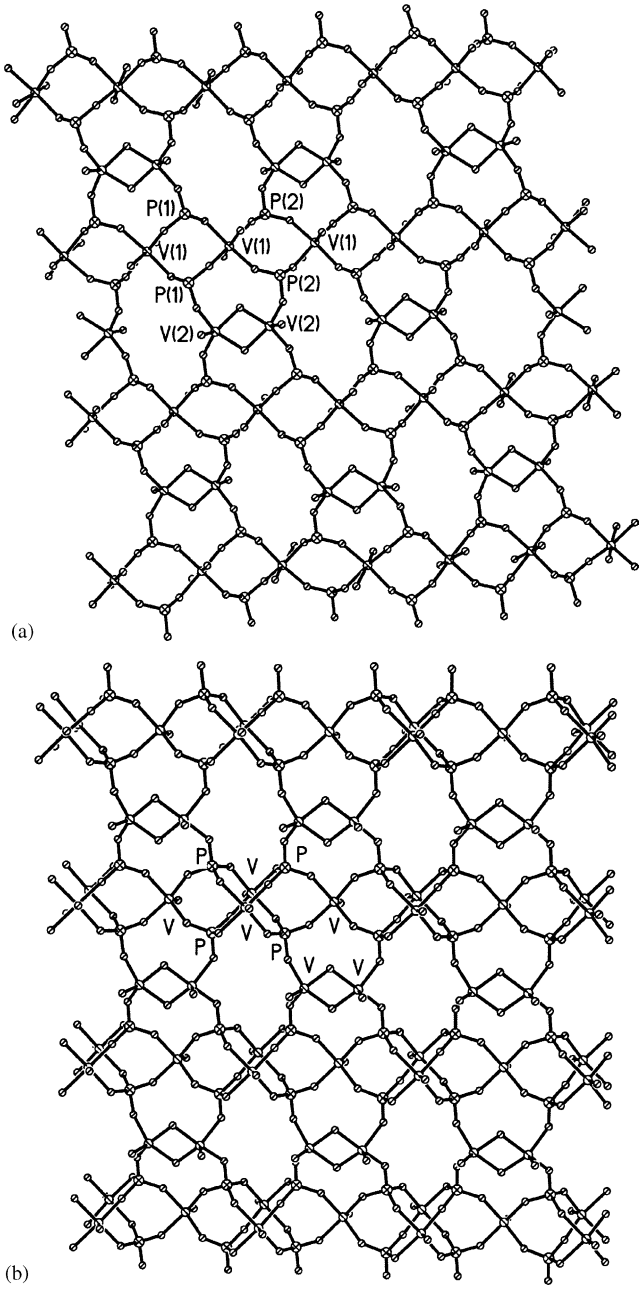

Fig. 4. (a) View of the V/P/O layer of the vanadium phosphite, $[HN(C_2H_4)_3N][(VO)_2(HPO_3)_2(OH)(H_2O)]\cdot H_2O$. (b) View of the V/P/O layer of the vanadium phosphate, $[(NH_3C_3H_6)NH(C_2H_4)_2NH(C_3H_6NH_3)][(VO)_5(OH)_2(PO_4)_4]\cdot 2H_2O$.

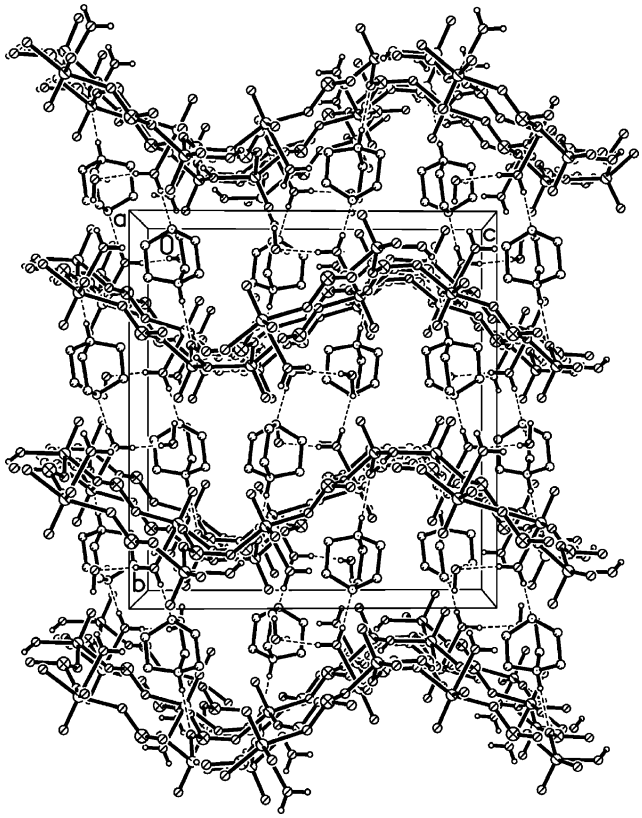

Fig. 5. View of the structure of the vanadium phosphite, along the *a*-axis. Dashed lines represent H bonds.

Table 4
Hydrogen bonds for $[HN(C_2H_4)_3N][(VO)_2(HPO_3)_2(OH)(H_2O)]\cdot H_2O$

D–H···A	d(D–H) (Å)	d(H···A) (Å)	d(D···A) (Å)	<(DHA) (°)
N(1)–H(1)···O(7)	0.83(12)	2.09(12)	2.913(7)	174(9)
O(5)–H(52)···N(2)#1	0.82(5)	1.95(5)	2.763(5)	169(10)
O(5)–H(51)···O(1W)#2	0.87(12)	2.09(12)	2.949(6)	169(9)
O(9)–H(9)···O(2)#3	0.87(12)	1.95(11)	2.765(5)	154(9)
O(9)–H(9) ···O(1)#3	0.87(12)	2.38(11)	3.012(4)	129(8)

Note. Symmetry transformations used to generate equivalent atoms: #1, $x+1/2$, $y+1/2$, z; #2, $-x+3/2$, $-y+1/2$, $-z+1$; #3, $-x+1$, y, $-z+1/2$.

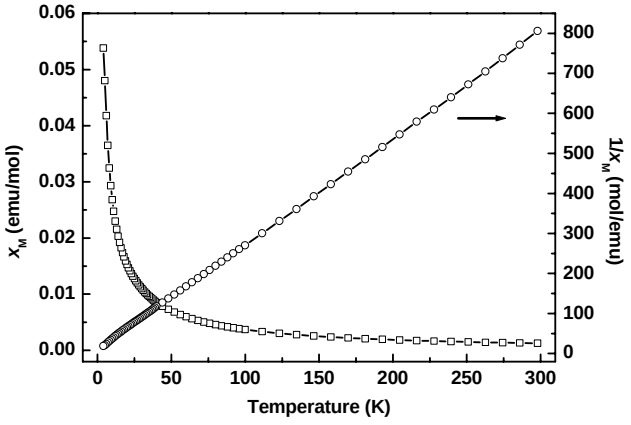

Fig. 6. Magnetic susceptibility and reciprocal susceptibility as a function of temperature for the vanadium phosphite.

μ_3-coordination mode, whereas the phosphate groups adopt the μ_4-coordination mode.

The H^+DABCO cations and water molecules occupy the void spaces between the $[(VO)(H_2O)(VO)(OH)(HPO_3)_2]^-$ layers, as depicted in Fig. 5. The structure contains an extended network of O–H···O, N–H···O and O–H···N hydrogen bonds, as listed in Table 4. The water molecule in the $[VO_5(H_2O)]$ octahedral forms hydrogen bonds with the "non-protonated" nitrogen atom in DABCO and O(1w) in interlamellar water molecule, respectively. The H^+DABCO cation is hydrogen bonded to the oxygen atoms (O(7)) in the $[(VO)(H_2O)(VO)(OH)(HPO_3)_2]^-$ layers. Thus, the H^+DABCO linkage involves an O(5)–H(52)···N(2)(C_2H_4)N(1)–H(1)···O(7) bridge, where O(5) is the water molecule attached to V(1), N(2) the "non-protonated" nitrogen atom of DABCO, N(1) the protonated nitrogen atom, and O(7) the atom in the $[(VO)(H_2O)(VO)(OH)(HPO_3)_2]^-$ layers.

3.3. Physical data

Magnetic susceptibility data for sample (Fig. 6) showed a paramagnetic behavior over the temperature range 4–298 K, with no evidence for any cooperative magnetic phenomenon. The measured data were fitted using the Curie–Weiss equation: $\chi_m = C_m/(T-\theta)$, where χ_m is the measured magnetic susceptibility, T the temperature (K), C_m the Curie constant and θ the Weiss constant, with $C_m = 2.6349\,\text{emu}\cdot\text{K}\cdot\text{mol}^{-1}$ and $\theta = -4.05$ K. At 298 K, the calculated effective magnetic moment per vanadium atom, determined from the equation $\mu_{\text{eff}} = 2.828(\chi_m T)^{1/2}$, is 1.72 μ_B, in good agreement with the predicted spin-only value of 1.73 μ_B for a d^1 vanadium (IV).

4. Conclusions

A novel layered inorganic–organic hybrid vanadium phosphite with the formula $[HN(C_2H_4)_3N][(VO)_2(HPO_3)_2(OH)(H_2O)]\cdot H_2O$ was synthesized under mild hydrothermal conditions. It was thermal stable below 300°C. The structure of the compound consists of the vanadium phosphite layers with composition of $[(VO)(H_2O)(VO)(OH)(HPO_3)_2]^-$, and water and H^+DABCO occupy in between the layers. The arrangement of these layers in the structure is wave like. The compound behaved paramagnetic over the temperature range of 4–298 K. The μ_3-coordination for the phosphites, which is different from the μ_4-coordination for the phosphites, presents further challenges in the hydrothermal synthesis of organically templated open-framework phosphites.

Acknowledgments

This work was supported by the National Natural Science Foundation of China (No. 20071013), the State Basic Research Project of China (G200077507) and Foundation for "Chang Jiang" scholarship by the Ministry of Education of China.

References

[1] A.K. Cheetham, G. Ferey, T. Loiseau, Angew. Chem. Int. Ed. 38 (1999) 3268.
[2] G. Ferey, Chem. Mater. 13 (2001) 3084.
[3] S. Fernandez, J.L. Pizarro, J.L. Mesa, L. Lezama, M.I. Arriortua, T. Rojo, Int. J. Inorg. Mater. 3 (2001) 331.

[4] S. Fernandez, J.L. Pizarro, J.L. Mesa, L. Lezama, M.I. Arriortua, R. Olazcuaga, T. Rojo, Inorg. Chem. 40 (2001) 3476.
[5] S. Fernandez, J.L. Mesa, J.L. Pizarro, L. Lezama, M.I. Arriortua, R. Olazcuaga, T. Rojo, Chem. Mater. 12 (2000) 2092.
[6] W.T.A. Harrison, Int. J. Inorg. Mater. 3 (2001) 187.
[7] J.A. Rodgers, W.T.A. Harrison, Chem. Commun. (2000) 2385.
[8] W.T.A. Harrison, M.L.F. Phillips, J. Stanchfield, T.M. Nenoff, Inorg. Chem. 40 (2001) 895.
[9] W.T.A. Harrison, J. Solid State Chem. 160 (2001) 4.
[10] W.T.A. Harrison, M.L.F. Phillips, T.M. Nenoff, J. Chem. Soc. Dalton Trans. (2001) 2459.
[11] W.T.A. Harrison, M.L.F. Phillips, T.M. Nenoff, Int. J. Inorg. Mater. 3 (2001) 1033.
[12] G. Bonavia, J. DeBord, R.C. Haushalter, D. Rose, J. Zubieta, Chem. Mater. 7 (1995) 1995.
[13] V. Soghomonian, Q. Chen, R.C. Haushalter, J. Zubieta, C.J. O'Connor, Science 259 (1993) 1596.
[14] T. Loiseau, G. Ferey, J. Solid State Chem. 111 (1994) 416.
[15] Z. Bircsak, A.K. Hall, W.T.A. Harrison, J. Solid State Chem. 142 (1999) 168.
[16] J. Do, R.P. Bontchev, A.J. Jacobson, J. Solid State Chem. 154 (2000) 514.
[17] V. Soghomonian, Q. Chen, Y.P. zhang, R.C. Haushalter, C.J. O'connor, C. Tao, J. Zubieta, Inorg. Chem. 34 (1995) 3509.
[18] M.I. Khan, L.M. Meyer, R.C. Haushalter, A.L. Schweitzer, J. Zubieta, J.L. Dye, Chem. Mater. 8 (1996) 43.
[19] Software packages SMART and SAINT, Siemens Analytical X-ray Instruments Inc., Madison, WI, 1996; SHELXTL, Version 5.1; Siemens Industrial Automation, Inc. Madison, WI, 1997.
[20] PowderCell for Windows, Version 2.4, Federal Institute for Materials Research and Testing, Berlin, Germany, 2000.
[21] I.D. Brown, R.D. Shannon, Acta Crystallogr. A 29 (1973) 266.
[22] I.D. Brown, D. Altermatt, Acta Crystallogr. B 41 (1985) 244.
[23] W.T.A. Harrison, S.C. Lim, J.T. Vaughey, A.J. Jacobson, D.P. Goshorn, J.W. Johnson, J. Solid State Chem. 113 (1994) 444.
[24] A. Le Bail, M.D. Marcos, P. Amoros, Inorg. Chem. 33 (1994) 2607.